

# DATA PROCESSING AND COMPACT REPRESENTATION OF MEASURED ISOTROPIC SPECTRAL BRDF

Huiying Xu

Department of Computer Sciences, Purdue University, West Lafayette, Indiana 47907, USA

Keywords: BRDF, Data processing, Representation.

Abstract: This paper presents the methods for both data processing and compact representation of measured isotropic spectral BRDF. For the data processing, we develop a numerical method for filtering the noises, re-sampling the data from non-uniform sampling to uniform sampling, and interpolation. For the compact representation, we propose a method to represent the spectral BRDF in both the spectral and spatial domains. In spectral domain, for each pair of the incident and outgoing directions, we represent the spectral BRDF with Fourier coefficients. In spatial domain, for all the outgoing directions of a given incident direction, we represent the same-order Fourier coefficients either directly using a linear combination of spherical harmonics or a linear combination of spherical harmonics and a Gaussian, depending on their angular dependencies. Three Gaussian expressions are presented. Numerical studies are given for a measured isotropic spectral BRDF.

## 1 INTRODUCTION

Characterizing light reflection from object surfaces is essential in many areas, such as computer graphics and visualization, image analysis, remote sensing, medical imaging, confocal microscopy imaging, computational simulation, nondestructive inspection, and etc. The surface light reflections are generally described by a bi-directional reflection distribution function (BRDF)

$$\rho(\theta_i, \varphi_i, \theta_o, \varphi_o, \lambda) = \frac{dL_o(\theta_o, \varphi_o, \lambda)}{L_i(\theta_i, \varphi_i, \lambda) \cos \theta_i d\Omega_i}, \quad (1)$$

which is the ratio of the reflected radiance  $dL_o$  in direction  $(\theta_o, \varphi_o)$  to the incident irradiance  $L_i \cos \theta_i d\Omega_i$  in solid angle  $d\Omega_i = \sin \theta_i d\theta_i d\varphi_i$  (Figure 1), and  $\lambda$  is the wavelength. The incident (or lighting) and outgoing (or viewing) directions are specified respectively using the angle pairs  $(\theta_i, \varphi_i)$  and  $(\theta_o, \varphi_o)$ .

Some analytic models have been developed to describe surface reflection behavior. However, the current analytic models were developed based on various assumptions so that they are not applicable for all kinds of surfaces. Alternatively, one may obtain the raw data of BRDFs from the experimental measurements. However, there are some problems with the raw data. First, the data has unavoidably involved the noises so that the data cannot be

directly used. Second, we cannot measure the raw data for arbitrary pair of incident and outgoing directions, so we need a method to accurately interpolate the unmeasured pairs from all the measured pairs. Third, the measured raw data is often non-uniformly sampled. However, in some cases the uniformly sampled data is necessary for practical application. Fourth, since a spectral BRDF is a five dimensional function, the storage of raw data unavoidably occupies a huge space.

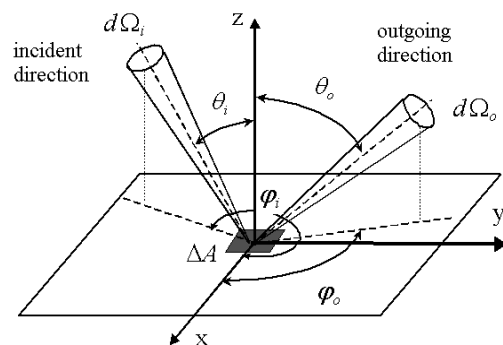


Figure 1: The geometry and notations of BRDF definition.

In this paper, we present the methods for both the data processing and compact representation. For the data processing, we developed a method to filter the noises involved in the raw data, resample the data, and interpolate it for the unmeasured pairs of

incident and outgoing directions. For the compact representation, we proposed a method to represent the spectral BRDF. In this method, for each pair of the incident and outgoing directions, we represent a BRDF with the Fourier coefficients. For all the outgoing directions of a given incident direction, we represent the same-order Fourier coefficients either directly using a linear combination of spherical harmonics or using a linear combination of spherical harmonics and a Gaussian, based on their angular dependencies. The reconstruction of spectral BRDF from representation just reverses this process.

This paper is organized as the follows. Section 2 reviews the background. Section 3 elaborates the data processing method. Section 4 describes the representation method. Section 5 presents the numerical studies. Section 6 gives the conclusions and future work.

## 2 BACKGROUND

Current analytic models commonly decompose the entire reflection into the diffuse and specular components. The diffuse component is typically assumed to be a Lambertian, but the specular component varies among models. A simple approach describes the specular component with the empirical functions (Phong, 1975; Strauss, 1990). More accurate models were developed from physically based approaches. One physically based approach uses Kirchoff theory with the tangent plane approximation (Beckmann, 1963). He et al. (1991) used this approach to model complex effects including light polarization, surface masking and shadowing, and subsurface scattering. Another approach is based on the Torrance-Sparrow microfacet model of surfaces (Torrance, 1967). This model assumes that a rough surface is comprised of many V-shaped planar, perfectly smooth, and isotropic microfacets. The specular component is expressed as a product of the Fresnel coefficient, the masking and shadowing factor, and the surface orientation probability, as presented in the Blinn-Cook-Torrance model (Blinn, 1977; Cook, 1982).

An early measurement of BRDFs used gonio-reflectometer (Murray-Coleman, 1990). However, the equipment is very expensive, and the measurement takes very long time. Ward (1992) introduced a novel device called imaging gonio-reflectometer. This system uses a half-silvered hemispherical mirror to collect the light from the sample surface and reflect it back into a CCD camera with a fisheye lens. This device is

inexpensive and the measurement is relatively faster. Dana et al. (1999) developed a simple system to measure bidirectional texture functions and BRDFs. Marschner et al. (1999, 2000) constructed a simple and rapid system to measure isotropic surfaces with spherical geometry. Matusik et al. (2003a, 2003b) developed a similar device and measured densely sampled BRDF data for different materials. Recently, Sun et al. (2005) measured some spectral BRDFs by the sample-rotated method. In which, the spectrum is captured by a PR-650 SpectraScan colorimeter. During the entire measurement, the colorimeter is fixed. Instead, the sample is rotated very often and the light source is relocated several times for all sampled incident and outgoing directions.

To save the storage space, it is desirable to represent the BRDF with fewer parameters. There are three popular representation methods. The first is representing a BRDF in terms of an empirical or physical model (Ward, 1992; Lafortune, 1997). This method is compact, but inaccurate. The second is representing a BRDF with a linear combination of a set of basis functions, such as spherical harmonics (Carbal, 1987; Sillion, 1991), Zernike polynomials (Koenderink, 1998), and wavelets (Schröder, 1995; Lalonde, 1997). The third is factoring a high-dimensional BRDF into a sum of low-dimensional functions (Fournier, 1995; DeYong, 1997). The second and third methods have the same problem: there exists a trade-off between the accuracy and compactness. For example, given a BRDF with the sensitive angular dependency, the larger number of coefficients is used, the more accurate the representation, but the less compact.

Most of the previous measurements and representations focused on the non-spectral BRDF (such as RGB-based). However, spectral BRDF offers the better commitment for faithful image rendering and analysis. Therefore, we need to develop the correspondent methods for the noises filtering, data re-sampling, data interpolation, and compact representation of measured spectral BRDF. All of these considerations ignite the current work.

## 3 DATA PROCESSING METHOD

The errors involved in the measurement of spectral BRDF are diversified. First, for different outgoing directions, the sample surface viewed by the colorimeter is different. The larger is the angle between the surface normal and outgoing direction, the larger is the area. Since the sample surface is not

strictly smooth and isotropic, the measured spectra must involve some errors. Second, since the sample, light source, and colorimeter are rotated or located manually, this can result in another kind of errors. Third, the unstable intensity of light source can also be a source of errors.

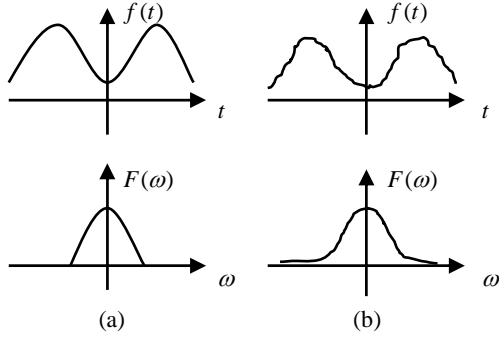


Figure 2: Fourier transformations of  $f(t)$  without noises (a) and with noises (b).

Generally, the contribution of experimental errors to the measured data oscillates quickly between the positive and negative effects. Therefore, we can regard them as the noises that are dominated by the high frequency components. Consider one-dimensional case, Fourier transformations of  $f(t)$  with and without the noises are shown in Figure 2. In the subfigure (a), we can find a cut-off frequency  $\omega_F$  so that  $F(\omega)=0$  for  $|\omega|>\omega_F$ . However, in the subfigure (b), it is difficult to find such a cut-off frequency since the noises contribute wide high frequency components to the spectrum  $F(\omega)$ . Therefore, to filter the noises, we can cut off the high frequency components with  $|\omega|>\omega_F$ , and perform inverse Fourier transformation to get the clean raw data, as shown in Figure 3.

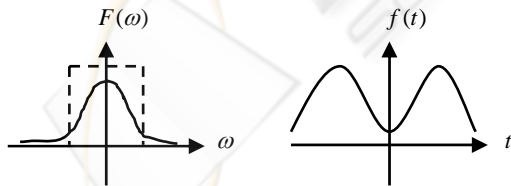


Figure 3: Inverse Fourier transformations for noises removing.

Given the one-dimensional function  $f(t)$ , the uniformly sampled data  $g(nT_0)$  with the period  $T_0$  can be expressed as (Glassner, 1995)

$$g(nT_0) = f(t) \sum_k \delta(t - kT_0). \quad (2)$$

The sampling process is shown in Figure 4.

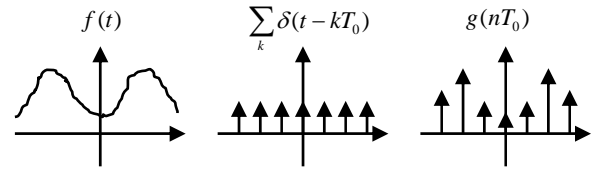


Figure 4: Illustration of uniform data sampling.

Using the property of convolution, Fourier transformation of the sampled data  $g(nT_0)$  is given as (Glassner, 1995)

$$G(\omega) = \frac{\kappa_T}{\kappa} \sum_k F(\omega - k\omega_0), \quad (3)$$

where  $\omega_0 = \frac{2\pi}{T_0}$ ,  $\kappa = \frac{1}{\sqrt{2\pi}}$ , and  $\kappa_T = \frac{1}{T_0}$ .  $G(\omega)$  is shown in Figure 5. We can see that, copies of  $F(\omega)$  overlap just a little for  $|\omega_0| > 2\omega_F$ , and quite a lot for  $|\omega_0| < 2\omega_F$ .

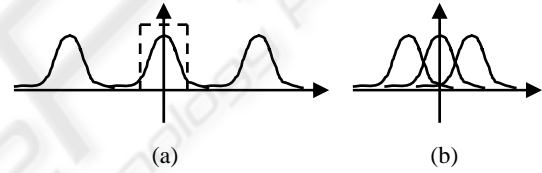


Figure 5: Illustration of  $G(\omega)$  for  $|\omega_0| > 2\omega_F$  (a) and  $|\omega_0| < 2\omega_F$  (b).

To filter the noises from  $f(t)$ , we need to sample the raw data with the period  $T_0$  so that  $|\omega_0| > \omega_F$ . Then we can multiply  $G(\omega)$  with a box spectrum  $B_{\omega_F}(\omega)$ , as dotted line shown in Figure 5(a). Finally we perform the inverse Fourier transformation to obtain the filtered  $f(t)$ . The one-dimensional expression is given as (Glassner, 1995)

$$f(t) = \sum_n g(nT_0) \text{sinc} \left[ \frac{\omega_F}{2\pi} (t - nT_0) \right]. \quad (4)$$

The isotropic BRDF can be described by a four-dimensional function with the parameters  $\lambda$ ,  $\theta_i$ ,  $\theta_o$ , and  $\varphi_o$ . Following Eqs. (2-4), the BRDF for each component of wavelength is given as

$$\rho_\lambda(\theta_i, \theta_o, \varphi_o) = \sum_m \sum_n \sum_l g_\lambda[m, n, l] \text{sinc} \left[ \frac{W_1}{2\pi} (\theta_i - mT_1) \right] \cdot \text{sinc} \left[ \frac{W_2}{2\pi} (\theta_o - nT_2) \right] \text{sinc} \left[ \frac{W_3}{2\pi} (\varphi_o - lT_3) \right] \quad (5)$$

where  $T_1$ ,  $T_2$  and  $T_3$  are the sampled periods for  $\theta_i$ ,  $\theta_o$  and  $\varphi_o$ , respectively,  $g_\lambda[m, n, l]$  is the uniformly

sampled data for the grid point ( $\theta_i = mT$ ,  $\theta_o = nT_2$ ,  $\varphi_o = lT_3$ ), and  $W_1 = \frac{2\pi}{T_1}$ ,  $W_2 = \frac{2\pi}{T_2}$ , and  $W_3 = \frac{2\pi}{T_3}$ .

Although the raw data of measured spectral BRDF is non-uniformly sampled and densely distributed, we can obtain the optimal solution  $g_\lambda[m, n, l]$  by solving the linear least squares problem

$$\min \left\| \rho_{raw} - \sum_m \sum_n \sum_l g_\lambda[m, n, l] \text{sinc} \left[ \frac{W_1}{2\pi} (\theta_i - mT_1) \right] \cdot \text{sinc} \left[ \frac{W_2}{2\pi} (\theta_o - mT_2) \right] \text{sinc} \left[ \frac{W_3}{2\pi} (\varphi_o - mT_3) \right] \right\|_2, \quad (6)$$

with the constraint  $g_\lambda[m, n, l] \geq 0$ . This constraint comes from the property that the reflectance is non-negative. We can implement the non-negative least squares (NNLS) algorithm (Lawson, 1995) to solve this constrained linear least squares problem.

For the outgoing directions perpendicular to the sample surface, the BRDF has the property:

$$\rho(\theta_i, 0, 0) = \rho(\theta_i, 0, T_3) = \dots = \rho(\theta_i, 0, lT_3). \quad (7)$$

In addition, the isotropic BRDF has the property:

$$\rho(0, \theta_o, 0, \lambda) = \rho(0, \theta_o, T_3, \lambda) = \dots = \rho(0, \theta_o, lT_3, \lambda). \quad (8)$$

Therefore, we renormalize the matrix in Eq. (6) so that the optimal solution still satisfies these properties. Assume that  $x_1 = x_2$  for the following linear least squares problem

$$\min \left\| \begin{pmatrix} a_{11} & a_{12} & a_{13} \\ a_{21} & a_{22} & a_{23} \\ a_{31} & a_{32} & a_{33} \end{pmatrix} \begin{pmatrix} x_1 \\ x_2 \\ x_3 \end{pmatrix} - \begin{pmatrix} b_1 \\ b_2 \\ b_3 \end{pmatrix} \right\|_2, \quad (8)$$

the matrix can be renormalized so that the linear least squares problem becomes

$$\min \left\| \begin{pmatrix} a_{11} + a_{12} & a_{13} \\ a_{21} + a_{22} & a_{23} \\ a_{31} + a_{32} & a_{33} \end{pmatrix} \begin{pmatrix} x_1 \\ x_3 \end{pmatrix} - \begin{pmatrix} b_1 \\ b_2 \\ b_3 \end{pmatrix} \right\|_2. \quad (9)$$

For the outgoing directions far away from the highlights, the BRDF varies smoothly and gradually. Hence, the raw data is usually captured sparsely. However, the sparse data can result in the failure of solving Eq. (6). To solve this problem, we introduce the following linear relations into the linear least squares problem

$$\begin{aligned} g_\lambda[m-1, n, l] - 2g_\lambda[m, n, l] + g_\lambda[m+1, n, l] &= 0 \\ g_\lambda[m, n-1, l] - 2g_\lambda[m, n, l] + g_\lambda[m, n+1, l] &= 0. \quad (10) \\ g_\lambda[m, n, l-1] - 2g_\lambda[m, n, l] + g_\lambda[m, n, l+1] &= 0 \end{aligned}$$

It is obvious that the optimal solution is uniformly sampled. To interpolate the BRDF for any unmeasured pair of incident and outgoing directions, we just need to follow Eq. (5).

## 4 REPRESENTATION METHOD

Our representation method consists of two stages. In the first, we represent the spectral BRDF in the spectral domain. In the second, we represent the Fourier coefficients in spatial domain.

### 4.1 Spectral Domain

For each pair of incident and outgoing directions, a spectral BRDF is a spectrum. Therefore, we perform Fourier transformation to it and represent it with Fourier coefficients. The expression is given as

$$\begin{aligned} \rho(\theta_i, \theta_o, \varphi_o, \lambda) &= \frac{1}{2} a_0(\theta_i, \theta_o, \varphi_o) \\ &+ \sum_{k=1} \left\{ a_k(\theta_i, \theta_o, \varphi_o) \cos \left[ \frac{2\pi k(\lambda - \lambda_{\min})}{\Delta\lambda} \right] \right. \\ &\left. + b_k(\theta_i, \theta_o, \varphi_o) \sin \left[ \frac{2\pi k(\lambda - \lambda_{\min})}{\Delta\lambda} \right] \right\} \end{aligned} \quad (11)$$

where  $\Delta\lambda = \lambda_{\max} - \lambda_{\min}$  is the visible range, and

$$\begin{aligned} a_k(\theta_i, \theta_o, \varphi_o) &= \frac{2}{\Delta\lambda} \int_{\lambda_{\min}}^{\lambda_{\max}} d\lambda \rho(\theta_i, \theta_o, \varphi_o, \lambda) \\ &\cdot \cos \left[ \frac{2\pi k(\lambda - \lambda_{\min})}{\Delta\lambda} \right], \quad k = 0, 1, K, \infty \\ b_k(\theta_i, \theta_o, \varphi_o) &= \frac{2}{\Delta\lambda} \int_{\lambda_{\min}}^{\lambda_{\max}} d\lambda \rho(\theta_i, \theta_o, \varphi_o, \lambda) \\ &\cdot \sin \left[ \frac{2\pi k(\lambda - \lambda_{\min})}{\Delta\lambda} \right], \quad k = 1, 2, K, \infty \end{aligned} \quad (12)$$

### 4.2 Spatial Domain

For all the outgoing directions of a given incident direction, we represent the same-order Fourier coefficients. If these coefficients have insensitive angular dependencies on the outgoing directions, we represent them directly using a linear combination of spherical harmonics. Otherwise, we decompose them into a smooth background and a sharp lobe. Since the smooth background is dominated by the low-frequency components, we can represent them efficiently using a linear combination of low-level spherical harmonics. The sharp lobe is dominated by the high-frequency components, so we represent it using a Gaussian. The decomposition is shown in Figure 6. For the  $k$ th Fourier coefficients, the representation is given as

$$\sum_{l=0}^L \sum_{m=-l}^l A_{k, (l, m)}(\theta_i) Y_{l, m}(\theta_o, \varphi_o) + G_k(\theta_i, \theta_o, \varphi_o). \quad (13)$$

Here the first term represents the smooth background,  $Y_{l, m}(\theta_o, \varphi_o)$  is the spherical harmonic with the level ( $l, m$ ),  $L$  the maximum level, and

$A_{k,(l,m)}(\theta_i)$  the coefficients. The second term  $G_k(\theta_i, \theta_o, \varphi_o)$  represents the sharp lobe, and it is a Gaussian.

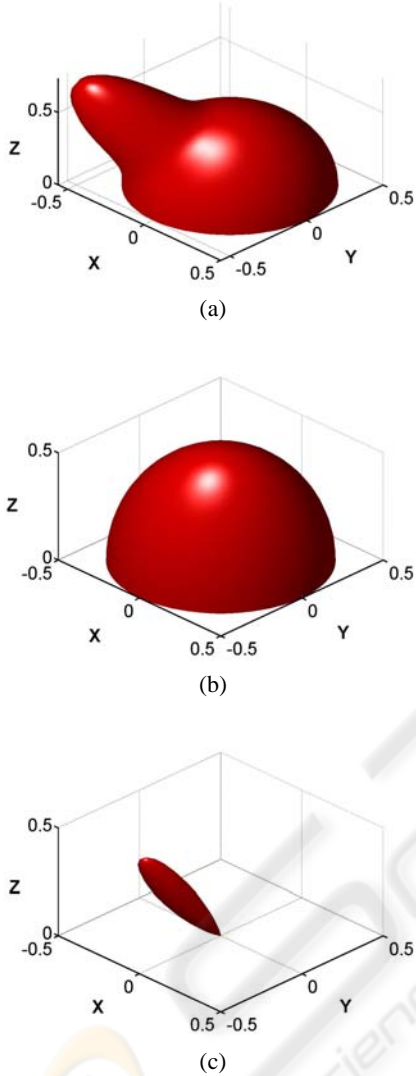


Figure 6: Decomposition of the same-order Fourier coefficients (a) into a smooth background (b) and a sharp lobe (c).

In this paper, we tried three Gaussians for the representation of the sharp lobe. The first is given as

$$G_k(\theta_i, \theta_o, \varphi_o) = p_k \exp[-\alpha_k^2(\theta_i, \theta_o, \varphi_o)/b_k], \quad (14)$$

where  $p_k$  and  $b_k$  specify the height and width of the sharp lobe, and  $\alpha_k(\theta_i, \theta_o, \varphi_o)$  is the angle between the outgoing direction  $(\theta_o, \varphi_o)$  and the direction of the peak of sharp lobe. For the isotropic spectral BRDF, the direction of the peak of sharp lobe is a function

of  $\theta_i$ . The second is generated from the empirical model (Ward, 1992)

$$G_k(\theta_i, \theta_o, \varphi_o) = p_k \exp[-\tan^2 \alpha_k(\theta_i, \theta_o, \varphi_o)/b_k], \quad (15)$$

and the third from the physically based model (Sun, 2004)

$$G_k(\theta_i, \theta_o, \varphi_o) = p_k \exp[-\tan \alpha_k(\theta_i, \theta_o, \varphi_o)/b_k]. \quad (16)$$

The decomposition of Fourier coefficients into a smooth background and a sharp lobe is a key point for this representation method. To achieve this, we need to obtain the critical angle first. Then, for all the outgoing directions with the angles from the peak of the sharp lobe are larger than the critical angle, we treat the Fourier coefficients as the smooth background. We can use the regression analysis (or linear least squares) to determine the coefficients  $A_{k,(l,m)}(\theta_i)$ . Finally, we extract the smooth background from the Fourier coefficients, and use the regression analysis (or linear least squares) to determine the coefficients  $p_k$  and  $b_k$ .

Finding the critical angle is a little tricky since we cannot directly obtain it from the raw data. In this paper, we first evaluate the range of critical angle from the raw data. Then we uniformly sample the range with a reasonable interval. For each sampled angle, we take it as the critical angle and use it for the decomposition. Correspondently we calculate the relative error between the raw data and the representation. Finally we select the sampled angle with the least relative error as the real critical angle.

## 5 NUMERICAL STUDIES

In this paper, the raw data of spectral BRDF is measured from a sample “ME01\_AmberGlass”. The data is non-uniformly sampled for the incident and outgoing directions in terms of the geometry of BRDF, and has the noises involved. Furthermore, the data is sparsely distributed around some pairs of incident and outgoing directions, while it is densely distributed around some other directions.

### 5.1 Data Processing

Following Eqs. (5-10), we obtain the uniformly sampled and noises-filtered spectral BRDF data. For different incident angle  $\theta_i$ , the spectral BRDF at  $\lambda = 550\text{nm}$  for different outgoing directions is shown in Figure 7. In this paper,  $\theta = -\phi$  stands for the outgoing direction  $(\phi, 0^\circ)$ , and  $\theta = \phi$  for

$(\phi, 180^\circ)$ . We can see that the BRDF shows apparent off-specular reflection for  $\theta_i = 15^\circ, 45^\circ$ . Moreover, the BRDF shows higher peak for normal incidence, and for the incidence close to the grazing direction.

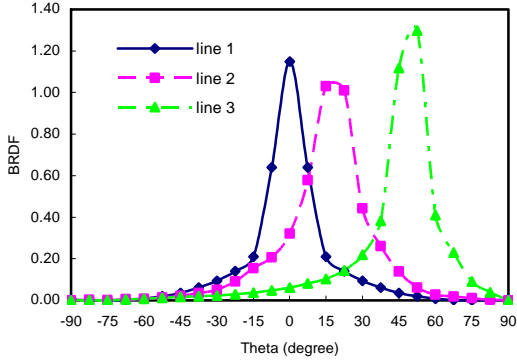


Figure 7: Spectral BRDF at  $\lambda = 550\text{nm}$  for  $\theta_i = 0^\circ$  (line 1),  $\theta_i = 15^\circ$  (line 2), and  $\theta_i = 45^\circ$  (line 3).

Following Eq. (5), we interpolate the spectral BRDF for the unmeasured pairs of incident and outgoing directions. By converting the spectra into the RGB color components, the BRDF for normal incidence is shown in Figure 8.

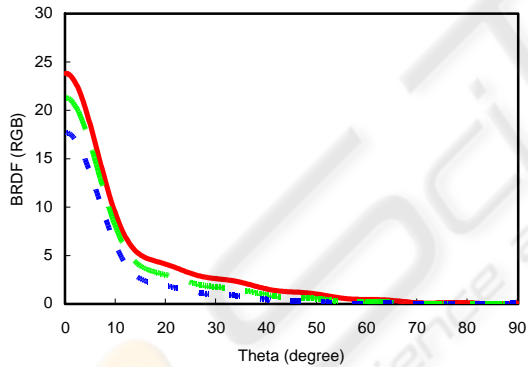


Figure 8: Interpolated BRDF for normal incidence.

From Figure 8, we can see some oscillations for  $10^\circ < \theta < 60^\circ$ . This phenomenon is commonly called the ring effect. It may come from two reasons. One is caused from the introduction of linear relations, as shown in Eq. (10), and another from the inherit ring effect of Eq. (5) (Glassner, 1995). To remove the ring effect, we multiply a window function  $w(m, n, l)$  to the right term of Eq. (5),

$$w(m, n, l) = \cos[2(\theta_i - mT_1)] \cdot \cos[2(\theta_o - nT_2)] \cos[2(\phi_o - lT_3)] \quad (17)$$

In calculation, we always take  $w(m, n, l) = 0$  if  $w(m, n, l) < 0$  for some cases. The interpolated BRDF with the ring effect removed is shown in Figure 9.

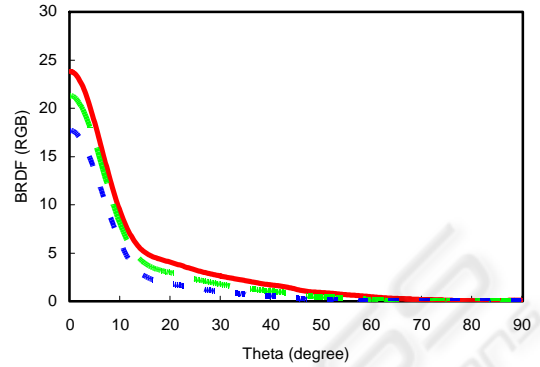


Figure 9: Interpolated BRDF with the ring effect removed for normal incidence.

## 5.2 Representation

The accuracy of a representation method can be evaluated in terms of the relative error between the reconstructed spectral BRDF and the original one

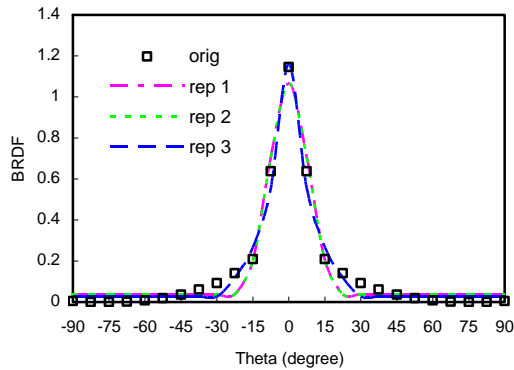
$$\eta = \sqrt{\frac{\sum_{\lambda} \sum_{\theta_o} \sum_{\phi_o} [\rho_{reconstr}(\theta_i, \theta_o, \phi_o) - \rho_{orig}(\theta_i, \theta_o, \phi_o)]^2}{\sum_{\lambda} \sum_{\theta_o} \sum_{\phi_o} [\rho_{orig}(\theta_i, \theta_o, \phi_o)]^2}} \quad (18)$$

where  $\rho_{reconstr}(\theta_i, \theta_o, \phi_o)$  and  $\rho_{orig}(\theta_i, \theta_o, \phi_o)$  are the reconstructed and original spectral BRDFs, respectively.

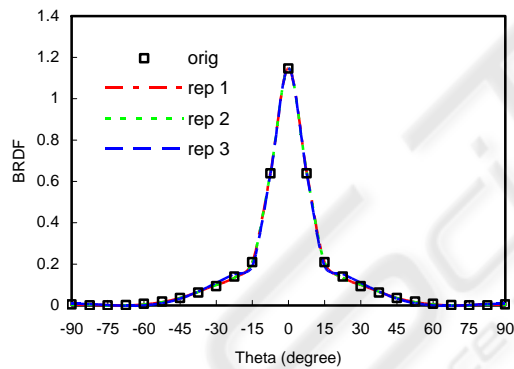
For the re-sampled and noises-filtered data, we represent the spectral BRDF for each pair of incident and outgoing directions with 19 Fourier coefficients, while the original data size is 101. Since the spectral BRDF is sensitively angular dependent, the same-order Fourier coefficients of each sampled incident direction is also highly angular dependent. We have to decompose the Fourier coefficients into a smooth background and a sharp lobe, and represent them respectively. For normal incidence, Figure 9 shows the comparisons between the original data and the ones reconstructed from the representations at  $\lambda = 550\text{nm}$ . Here, the line “orig” stands for the original data, the line “rep 1” for the representation using Eq. (14), the line “rep 2” for that using Eq. (15), and the line “rep 3” for that using Eq. (16).

For  $L=1$ , as shown in Figure 9(a), the representation error for the representation using either Eq. (14) or Eq. (15) is 14.3%, and that using Eq. (16) is 11.5%. From Figure 9(a), we can see that the representation error mainly comes from the

representation for the smooth background; this is due to the fact that the low-level spherical harmonics cannot represent the high-frequency components completely. Moreover, we can see that the representation using Eq. (16) matches the sharp lobe of the original data better than the representations using Eq. (14) and Eq. (15). This fact indicates that the physical model (Sun, 2004) might match the original data better than the empirical model (Ward, 1992).



(a)



(b)

Figure 10: Comparisons between the original data and the representations for normal incidence.

For  $L=4$ , as shown in Figure 9(b), the representation error for using each of Eqs. (14-16) is lower than 4.5%. Here, the total number of coefficients used for representation is  $(25+2) \times 19$ . Consider the size of the original data size  $13 \times 49 \times 101$  for each incident direction, in which the sample interval for all the angles is 7.5 degrees, the compression ratio is 125:1.

To understand how well the representations match the original data for full range of wavelength, we compare the original data with the representations for the normal incidence and the

outgoing direction  $(0^\circ, 0^\circ)$ , as shown in Figure 10. We can see that the representation error mainly comes from the two bottoms of full range of wavelength. This is due to the property of Fourier transformation; the representation always starts and ends with the same value.

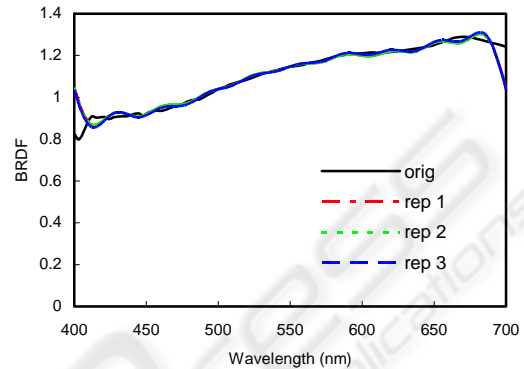


Figure 11: Comparisons between the original data and the representations for full range of wavelength.

## 6 CONCLUSIONS AND FURTHER WORK

In this paper, we present the methods for both data processing and compact representation of the measured isotropic spectral BRDF. For the data processing, we develop a numerical method to filter the noises and resample the raw data by solving a constrained linear least squares problem, and interpolate the processed data for the unmeasured pair of incident and outgoing directions from the measured pairs. Numerical results show that the interpolated spectral BRDF has the ring effect, which might cause from the introduction of linear relations into the matrix for linear least squares analysis and the inherit ring effect. By introducing a window function into the interpolation, the ring effect is remarkably reduced.

For the compact representation of processed data, we develop a method to represent the data in both the spectral and spatial domains. In the spectral domain, for each pair of the incident and outgoing directions, we consider it as a spectrum, and represent it with the Fourier coefficients by performing the Fourier transformation to it. For all the outgoing directions of a given direction, we consider the same-order Fourier coefficients. If these coefficients are insensitively angular dependent, we represent them directly using a linear combination of

spherical harmonics. Otherwise, we decompose them into a smooth background and a sharp lobe; we represent the smooth background using a linear combination of spherical harmonics, and the sharp lobe using a Gaussian. Numerical studies show that, for the measured isotropic spectral BRDF of a sample, the representation error can be lower than 4.5% by using  $L=4$  and the number of Fourier coefficients 19. The compression ratio is achieved as 125:1.

In further work, we will continue to work on representing the processed data for an arbitrary incident direction. We will use both the processed data and represented data for the spectral imaging and give the comparisons. Furthermore, we will measure the spectral BRDFs for different surfaces, and use these methods for data processing and representation. Once the data is processed, we will compare it with the current analytic models for the full range of wavelength, and find the hiding problems with them. Based on the comparisons, we can work on developing the new analytic models.

## ACKNOWLEDGEMENTS

The author thanks Yinlong Sun for providing the spectral BRDF of the sample "ME01\_AmberGlass".

## REFERENCES

- Beckmann, P., & Spizzichino, A., 1963, *The scattering of electromagnetic waves from rough surfaces microform*, Macmillan, New York.
- Blinn, J. F., 1977, Models of light reflection for computer synthesized pictures, *Proc. Siggraph*, pp. 192-198.
- Carbral, B., Max, N., & Springmeyer, R., 1987, Bidirectional reflection functions from surface bump maps, *Computer Graphics*, vol. 21, no. 4, pp. 273-281.
- Cook, R. L., & Torrance, K. E., 1982, A reflection model for computer graphics, *ACM Transactions on Graphics*, vol. 1, no. 1, pp. 7-24.
- Dana, K. J., van Ginneken B., Nayar, S. K., & Koenderink, J. J., 1999, Reflectance and texture of real-world surfaces, *ACM Transactions on Graphics*, vol. 18, no. 1, pp. 1-34.
- DeYong, and Fourier A., 1997, Properties of tabulated bi-directional reflectance distribution functions, *Proc. Graphics Interface*, pp. 47-55.
- Fournier, A., 1995, Separating reflection functions from linear radiosity, *Proc. Eurographics Workshop on Rendering*, pp. 296-305.
- Glassner, A. S., 1995, *Principles of Digital Image Synthesis*, Morgan Kaufmann Publishers, San Francisco, CA.
- He, X. D., Torrance, K. E., Sillion, F. X., and Greenberg, D. P., 1991, A comprehensive physical model for light reflection, *Proc. Siggraph*, pp. 175-186.
- Koenderink, J. J., & van Doorn A. J., 1998, Phenomenological description of bi-directional surface reflection, *J. Opt. Soc. Am. A.*, vol. 15, no. 11, pp. 2903-2912.
- Lafortune, E. P. F., Foo, Sing-Choong, Torrance, K. E., Greenberg, D. P., 1997, Non-linear approximation of reflectance functions, *Proc. Siggraph*, pp. 117-126.
- Lawson, C. L., & Hanson, R. J., 1995, *Solving Least Squares Problems*, Philadelphia: SIAM.
- Marschner, S. R., Westin, S. H., Lafortune, E. P. F., Torrance, K. E., & Greenberg, D. P., 1999, Image-based BRDF measurement including human skin, *Proc. Euro-graphics Workshop on Rendering*, pp. 139-152.
- Marschner, S. R., Westin, S. H., Lafortune, E. P. F., & Torrance, K. E., 2000, Image-based measurement of the bi-directional reflection distribution function, *Applied Optics*, vol. 39, no. 16, pp. 2592-2600.
- Murray-Coleman, J. F., & Smith, A. M., 1990, The automated measurements of BRDFs and their applications to luminaire modelling, *Journal of the Illumination Engineering Society*, vol. 19, no. 1, pp. 87-89.
- Phong, B., 1975, Illumination for computer generated images, *Communications of the ACM*, vol. 18, no. 6, pp. 311-317.
- Schröder, P., & Sweldens, W., 1995, Spherical wavelets: efficiently representing functions on the sphere, *Computer Graphics*, vol. 29, pp. 161-172.
- Sillion, F. X., Arvo, J. R., Westin, S.H., and Greenberg, D. P., 1991, A global illumination solution for general reflectance distributions, *Computer Graphics*, vol. 25, no. 4, pp. 187-196.
- Strauss, P., 1990, A realistic lighting model for computer animators, *IEEE Computer Graphics & Appl.*, vol. 10, no. 6, pp. 56-64.
- Sun, Y., 2004, Self shadowing and local illumination of randomly rough surfaces, *Proc. CVPR*, pp. 158-165.
- Sun, Y., & Wang, Q., 2005, Spectral BRDF measurement and data interpolation, *Proc. of the 13th Color Imaging Conference*, pp. 114-119.
- Torrance, K. E., & Sparrow, E. M., 1967, Theory for off-specular reflection from roughened surfaces, *J. Opt. Soc. Am.*, vol. 57, no. 9, pp. 1105-1114.
- Ward, G. J., 1992, Measuring and modelling anisotropic reflection, *Proc. Siggraph*, pp. 265-272.